Spatiotemporal shaping of half-cycle terahertz pulses by diffraction through conductive apertures of finite thickness

Jake Bromage, Stojan Radic, G. P. Agrawal, and C. R. Stroud, Jr.

The Institute of Optics and Rochester Theory Center, University of Rochester, Rochester, New York 14627

P. M. Fauchet and Roman Sobolewski

Department of Electrical Engineering and Laboratory for Laser Energetics, University of Rochester, Rochester, New York 14627

Received June 3, 1997; revised manuscript received September 2, 1997

We demonstrate a simple quasi-optical technique for spatiotemporal shaping of half-cycle terahertz-radiation pulses. We show, both experimentally and theoretically, that properly polarized half-cycle pulses can be modulated temporally by diffraction through a conductive aperture of finite thickness. We use the finite-difference time-domain method to solve Maxwell's equations for such a geometry and show that it can explain all the experimentally observed features. In the case of a thick aperture, a planar waveguide model can also be used to describe the propagation of the pulse through the aperture, with excellent agreement with the experimental results. © 1998 Optical Society of America [S0740-3224(98)03903-4]

OCIS codes: 080.0080, 320.5540, 050.1220, 320.5550.

1. INTRODUCTION

Techniques for generation of ultrafast optical pulses have advanced considerably during the past decade.[1,2] The shortest optical pulses generated to date are less than 5 fs wide[1] and are thus approaching the definition of subcycle radiation. A particularly interesting form of subcycle optical radiation is a half-cycle pulse. Ideally, one creates a half-cycle pulse by limiting the duration of a perfect harmonic wave to half of its optical period. The spectrum of such a half-cycle pulse, however, includes a strong dc component that does not propagate. We use the term "half-cycle" to refer to a pulse that has most of the propagating energy in the initial half-cycle. A host of applications that require an ultrawideband (UWB) spectrum will benefit from the half-cycle optical generation: These applications include time-domain spectroscopy, ultrafast imaging, and remote optical sensing. Although subcycle optical generation is yet to be demonstrated, half-cycle pulse generation in the millimeter domain [also known as terahertz (THz) radiation] is well established.[3–9] Starting with the pioneering research on the Hertzian dipole,[3] a number of methods for the generation of THz radiation have been developed. Most of these techniques use a photoconductive antenna approach in which an ultrashort optical pulse is incident upon a strongly biased semiconducting material (such as GaAs, InP, or CdTe) or radiation-damaged silicon-on-sapphire. Generated carriers are rapidly accelerated in the external (bias) field, producing a burst of THz radiation. Various antenna geometries have been employed to optimize both the radiated power and the pulse shape.[4,5] The presence of strong external bias is not essential for THz generation.[6] Other methods that use heterostructures, such as p-i-n junctions[7] and strained superlattices,[8] have also been demonstrated. In addition, a particularly interesting method for the generation of tunable THz radiation was recently reported[9]: A self-delayed, frequency-chirped ultrafast optical pulse is heterodyned in a photoconductor antenna to generate a frequency-tunable THz pulse.

A steady refinement of THz generation techniques has made several important applications possible, including time-domain far-infrared spectroscopy,[10] THz imaging,[11] control of Rydberg atoms,[12] and UWB ranging.[13] Many of these applications require a specific pulse shape, which can be obtained through either application-oriented pulse generation or postgeneration pulse processing. Frequency-dependent attenuation across the near-continuum spectra of half-cycle pulses leads to a strong spatiotemporal shaping during propagation. This effect was recently studied in the case of free-space propagation[14] as well as in the case of propagation through refractive (focusing) optical systems.[15] An additional motivation for the study of half-cycle shaping techniques is provided by the anticipated arrival of half-cycle optical sources.

Current spatiotemporal shaping techniques can be classified as either active (direct) or passive (quasi-optical). Active spatial control requires a radiating array that can be addressed either optically or electronically.[16] Passive techniques use quasi-optical elements that are either refractive (dielectric lens, prism) or diffractive (grating).[17]

In this paper we introduce a simple and elegant quasi-optical technique for spatiotemporal shaping of half-cycle THz radiation based on the use of conductive apertures of finite thickness. We show that a thick conductive aper-

0740-3224/98/071953-07$15.00

ture plays the role of a highly discriminative high-pass filter for a properly polarized half-cycle pulse. Aperture thickness, width, and incident pulse polarization are used to control precisely the shape of the diffracted THz radiation. Different experimental geometries are accurately modeled and discussed by use of a finite-difference time-domain (FDTD) Maxwell solver, providing detailed insight into the spatiotemporal dynamics of half-cycle pulse shaping. A simple waveguide model is developed and used to describe the observed temporal shaping. We show how this model can be used for synthesizing arbitrary high-pass filters.

2. EXPERIMENT

The experimental configuration is shown in Fig. 1(a). Both the emitter (E) and the detector (D) of the THz radiation were large-aperture photoconductive antennas.[18] We made the emitter by using a semi-insulating GaAs wafer oriented along the ⟨100⟩ plane. It had a cross-section area of 1 cm^2 and was biased with a field of 2 kV/cm by means of parallel Au–Ge–Ni electrodes. A 150-fs optical pulse obtained from an 810-nm Ti:sapphire laser triggered the THz emission by uniformly illuminating the GaAs wafer with a fluence of 20 $\mu J/cm^2$. The detector was fabricated by deposition of parallel Au–Ge–Ni electrodes, spaced 2 mm apart, upon an epilayer of low-temperature molecular beam epitaxy–grown GaAs (LT-GaAs).[18] The 1.5-μm-thick LT-GaAs layer was grown at 200 °C and annealed *in situ* at 600 °C to produce a short carrier lifetime of ~1 ps. A delayed Ti:sapphire pulse gated the detector by uniformly illuminating the 2-mm^2 active area with a fluence of 0.5 mJ/cm^2. When the optical and the THz pulses were present in the LT-GaAs at the same time, the carriers produced by the optical pulse were accelerated by the electric field of the THz pulse. The component of the THz field perpendicular to the detector electrodes caused a current to flow in the external circuit. We measured this small current (~1 pA) by chopping the 1-kHz optical pulse train that triggered the emitter and using a lock-in amplifier. We sampled the THz pulse electric field with a resolution that was limited to 600 fs by the lifetime of the carriers in the LT-GaAs.

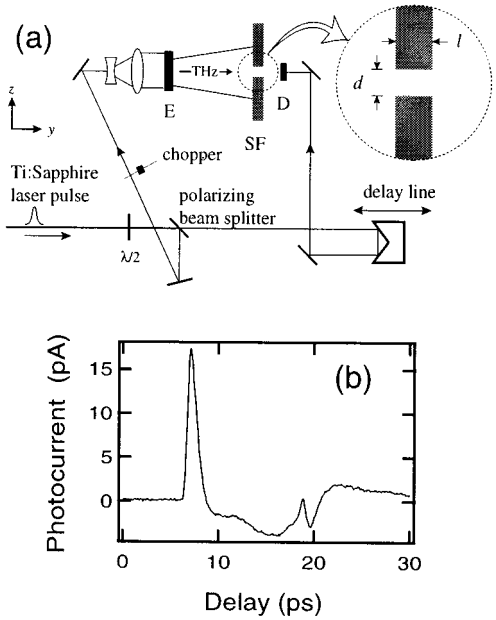

Fig. 1. (a) Experimental setup and (b) measured THz pulse incident upon the conducting aperture.

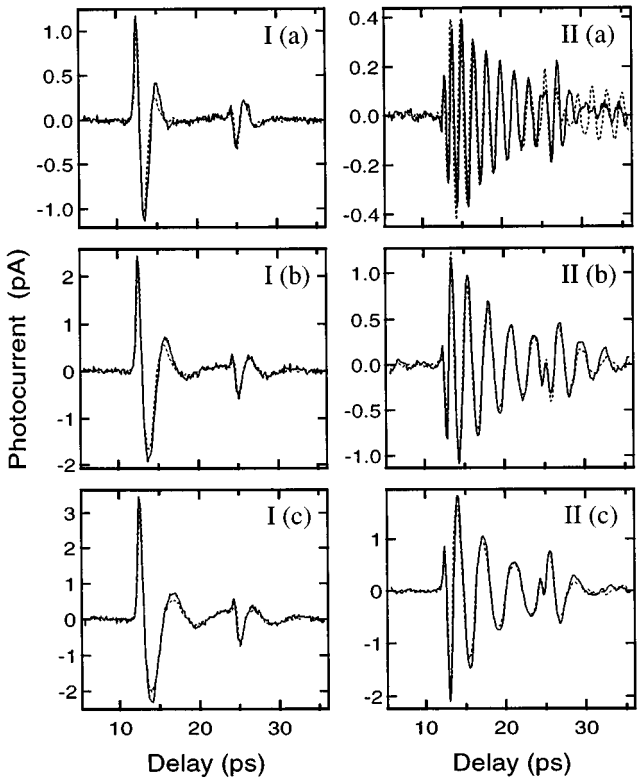

Fig. 2. Measured (solid curves) and FDTD calculated THz pulse shapes for thin (left) and thick (right) apertures: (a) 300-μm, (b) 500-μm, (c) 700-μm widths.

The adjustable slit filter (SF) was formed between the edges of two 5 cm × 10 cm sheets of copper, oriented parallel or perpendicular to the direction of THz polarization. The slit was 10 cm from the emitter, ensuring an approximately planar wave front over the slit widths of interest (0.1–5 mm). The incident THz pulse shown in Fig. 1(b) was measured 7 mm in front of the slit. Its main peak has a width (FWHM) of 1.3 ps and contains 72% of the detected energy. The small feature ~12 ps after the main peak is due to reflections within the 0.5-mm-thick emitter. The power spectrum of the pulse is peaked at 0.2 THz and extends past 1 THz.

We measured the effect of two types of slit filter in the two cases in which the thickness of the screen, l, was much less, or greater, than the cutoff wavelength. To make a slit filter in a screen whose thickness l is much less than the shortest wavelength of the THz pulse (1 THz ≡ 300 μm) we mounted razor blades on the inner edges of the copper sheets. To make a thick filter (i.e., a slit in a thick screen), we used a slit formed between 1.7-mm-thick copper sheets. By adjusting the slit width d we changed the shape of the transmitted pulses measured 7 mm after the filter. For slit widths $d \sim 1$ mm, the pulses transmitted by the thick and the thin filters are dramatically different, as shown in Fig. 2. Note that the

pulse transmitted by the thick filter is chirped and oscillates with a period that decreases as the slit width decreases.

3. FINITE-DIFFERENCE TIME-DOMAIN NUMERICAL SIMULATION

In this section we discuss the results of numerical simulations performed by the FDTD method. Assume a two-dimensional scattering geometry, as shown in Fig. 3 (inset): the conductive aperture is oriented along the x axis, whereas the incident field travels along the y axis. Two distinct polarization modes are considered in this analysis: (a) the incident electric field is parallel to the conductive slit (z polarized) and (b) the incident electric field is orthogonal to the conductive slit (x polarized). The former case is referred to as TM polarizations and the latter corresponds to TE polarization. The two-dimensional space is divided into scattered and incident regions. The conductive aperture, the detector, and the space between them belong to the scattered region. A perfect plane wave is generated in the incident region, positioned in front of the aperture. The relatively small curvature of the actual incident THz pulse ($\sim$0.003 rad) allows for the perfect plane-wave approximation to be made. The calculation used the measured THz pulse shape [Fig. 1(b)] as the input to the FDTD algorithm. The calculated field is effectively terminated at the scattered domain boundaries by implementation of the Engquist–Majda conditions.[19] These conditions were successfully tested against a large computing domain in which no waves reflected from boundaries were allowed into the region between the aperture and the detector.

The copper aperture was modeled as a perfect electrical conductor (PEC). The PEC model is justified by the high conductivity of the copper used in the experiment ($\sigma \sim 6 \times 10^8$ [υ/m]). Inasmuch as the entire modeling domain consists of vacuum and PEC structures only, we

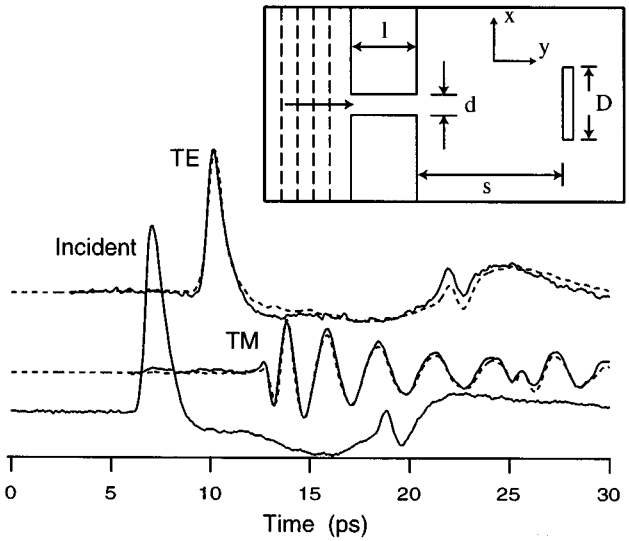

Fig. 3. Diffraction from a conductive slit: FDTD (dashed curves) versus measured (solid curves) field. The scattering geometry (inset) is defined by $d = 0.5$ mm, $D = 3$ mm, $s = 7$ mm, and $l = 1.7$ mm. The incident pulse shape (measured) is used in all subsequent FDTD simulations.

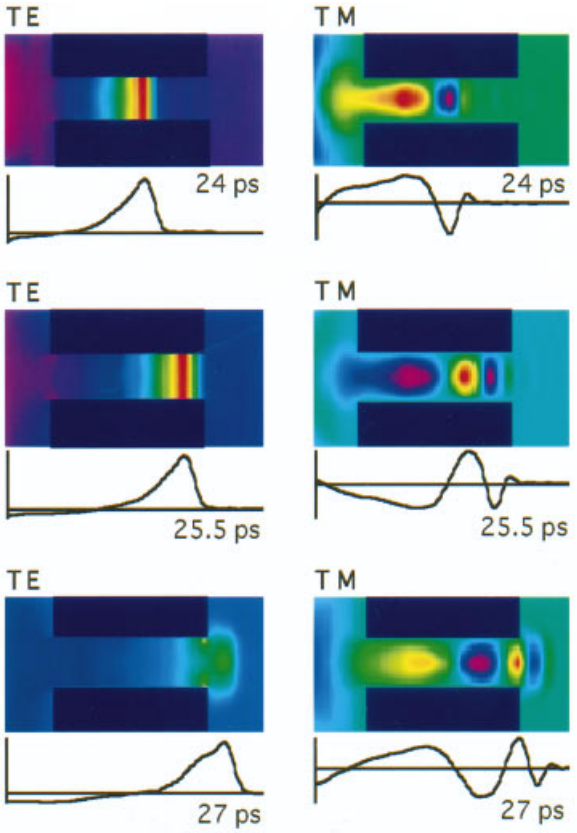

Fig. 4. TE (left) versus TM diffraction: Pulse propagation is tracked as it penetrates the aperture in time increments of 1.5 ps. The solid curves are the on-axis pulse profiles.

used a linear, nondispersive FDTD algorithm[19] in both the TM and the TE cases. The following set of FDTD equations was used to analyze TM scattering problem:

$$H_x^{n+1/2}(i, j + 1/2) = H_x^{n-1/2}(i, j + 1/2) + \frac{\Delta t}{\mu(i, j + 1/2)\Delta L} \times [E_z^n(i, j) - E_z^n(i, j + 1)], \quad (1)$$

$$H_y^{n+1/2}(i + 1/2, j) = H_y^{n-1/2}(i + 1/2, j) + \frac{\Delta t}{\mu(i + 1/2, j)\Delta L} \times [E_z^n(i + 1, j) - E_z^n(i, j)], \quad (2)$$

$$E_z^{n+1}(i, j) = E_z^n(i, j) + \frac{\Delta t}{\varepsilon(i + 1/2, j)\Delta L} [H_y^{n+1/2}(i + 1/2, j) - H_y^{n+1/2}(i - 1/2, j) + H_x^{n+1/2}(i, j - 1/2) - H_x^{n+1/2}(i, j + 1/2)], \quad (3)$$

where $x = i\Delta L$, $y = j\Delta L$, μ is the magnetic permeability, ε is the dielectric permittivity, ΔL is the spatial grid cell, and Δt is the time grid cell. Similarly, the TE diffraction problem is solved by use of the following set of equations:

$$E_x^{n+1}(i + 1/2, j) = E_x^n(i + 1/2, j) + \frac{\Delta t}{\varepsilon(i + 1/2, j)\Delta L} \times [H_z^{n+1/2}(i + 1/2, j + 1/2) - H_z^{n+1/2}(i + 1/2, j - 1/2)], \quad (4)$$

$$E_y^{n+1}(i, j + 1/2) = E_y^n(i, j + 1/2) + \frac{\Delta t}{\varepsilon(i, j + 1/2)\Delta L} \times [H_z^{n+1/2}(i - 1/2, j + 1/2) - H_z^{n+1/2}(i + 1/2, j + 1/2)], \quad (5)$$

$$H_z^{n+1/2}(i + 1/2, j + 1/2) = H_z^{n-1/2}(i + 1/2, j + 1/2) + \frac{\Delta t}{\mu(i + 1/2, j + 1/2)\Delta L} [E_x^n(i + 1/2, j + 1) - E_x^n(i + 1/2, j) + E_y^n(i, j + 1/2) - E_y^n(i + 1, j + 1/2)]. \quad (6)$$

An isotropic ($\Delta x = \Delta y = \Delta L = 15\ \mu$m) spatial grid was used in both the TM and the TE cases. The shortest wavelength present in the pulse spectrum ($\lambda \sim 300\ \mu$m) is resolved with an accuracy of $\lambda/20$, which dictates the spatial cell size to be $\Delta\lambda = 15\ \mu$m. To preserve the stability of the algorithm[20] the temporal step is set to $\Delta t = \Delta x/2c = 25$ fs. We estimate that the spatiotemporal grid described here induces a maximum propagation error of approximately 10^{-4}, as given by the phase-velocity relation[20] $v_P/c \sim \pi\Delta L/\{\lambda \sin^{-1}[2 \sin(\pi\Delta L/2\lambda)]\}$.

Figure 3 illustrates the accuracy of the FDTD method. Identical geometries are analyzed for both TE and TM cases: The detector is placed 7 mm away from a 500-μm-wide and 1.7-mm-thick PEC aperture. The finite size of the detector requires spatial averaging across its surface ($D = 3$ mm). Nevertheless, both calculated and measured diffracted waveforms serve as a good approximation for the on-axis field strength, as the detector subtends only $\pm 12°$ as viewed from the aperture. The extremely good agreement between the FDTD calculation and the measured data is apparent in Fig. 2, where diffracted waveforms are plotted for the thin and the thick TM cases. In the thin TM case (diffraction by a slit made from razor blades) the PEC aperture is modeled by two infinitely thin conductive sheets. Note that no scaling parameters have been used in comparing experimental and theoretical results.

It is clear from both the experimental results and the FDTD calculations that significant pulse reshaping occurs only in the case of thick-aperture TM diffraction. Figure 4 provides insight into the pulse formation within the thick aperture for the cases of negligible reshaping (TE) and strong pulse reshaping (TM). Dispersion-free propagation of the TE-polarized pulse is observed throughout the entire diffraction process. The TM-polarized pulse, on the other hand, is strongly dispersed and undergoes a complex temporal modulation as it penetrates the aperture.

4. ANALYTICAL WAVEGUIDE MODEL

Temporal modulation of half-cycle radiation diffracted by a thick TM aperture, as shown both experimentally and by FDTD simulations, represents the strongest shaping mechanism observed here. This conclusion appears to be valid for any diffracted direction and not only for the measured on-axis field, as we discuss below by using the FDTD method. Because the diffraction of the pulse by the conductive aperture is a linear process, it is natural to consider the problem in the frequency domain to gain further insight.

Consider the aperture transfer function, shown in Fig. 5 and measured experimentally. We plot the transfer function $T(\nu) = E_{\mathrm{IN}}(\nu)/E_{\mathrm{OUT}}(\nu)$ for a 1.7-mm-thick and 500-μm-wide aperture for the TM case by calculating the Fourier transform of the measured incident $[E_{\mathrm{IN}}(\nu)]$ and the transmitted $[E_{\mathrm{OUT}}(\nu)]$ on-axis THz pulses. The filter function describing the effect of the aperture exhibits a strong high-pass cutoff near 0.3 THz and a 6-dB transmission bandwidth of approximately 37 GHz. The nonlinear nature of the filter phase response is responsible for the strong dispersion observed in diffracted pulses, shown in Figs. 2 and 3. These results suggest a simple modeling approach in which a single-mode waveguide is formed between the faces of the conductive aperture.

Consider a waveguide that matches the aperture geometry by its length l and width d. It can be shown that the propagation constant of the mode propagating in this structure is[21]

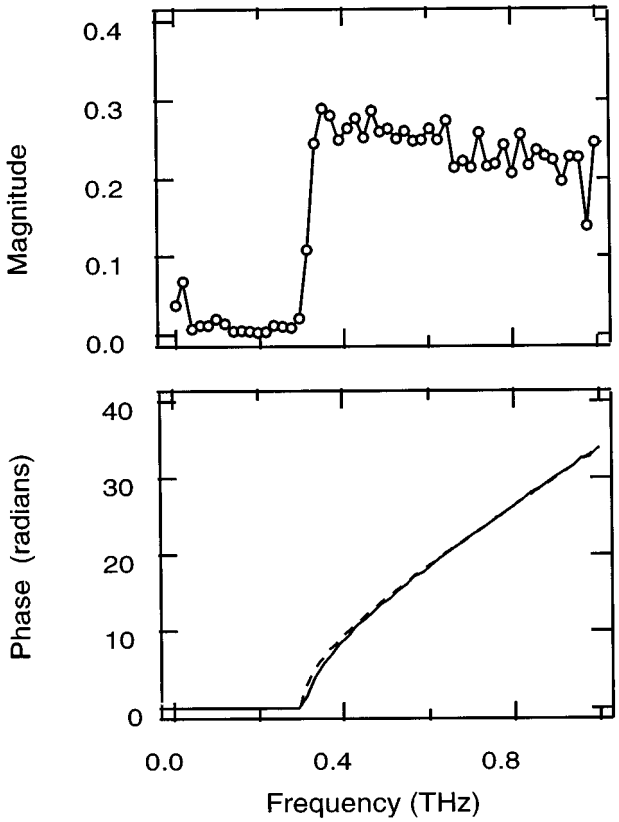

Fig. 5. Measured slit transfer function ($d = 0.5$ mm). Dashed curve, phase as predicted by the waveguide model.

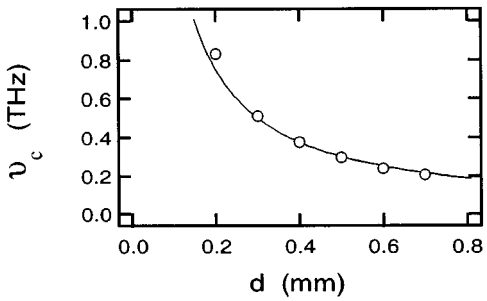

Fig. 6. Cutoff frequency for the thick conductive slit with TM polarization: waveguide prediction (solid curve) versus measured cutoff frequencies (points).

$$\beta(\nu) = \begin{cases} \dfrac{\pi}{d}\left[(\nu/\nu_c)^2 - 1\right]^{1/2} & \nu > \nu_c \\ i\,\dfrac{\pi}{d}\left[1 - (\nu/\nu_c)^2\right]^{1/2} & \nu \leqslant \nu_c \end{cases}, \tag{7}$$

where $\nu_c = c/2d$ is the cutoff frequency of the filter. The transfer function of the waveguide is given by $T(\nu) = \exp[i\beta(\nu)l]$. Figure 5 compares the predictions of the waveguide mode with the experimental data by plotting the phase of $T(\nu)$. The amplitude transmission above the cutoff frequency is 0.3, which we could easily increase by collimating the transmitted radiation with a standard silicon lens after it emerges from the waveguide.

Finally, in Fig. 6, where the dependence of the cutoff frequency (ν_c) on the waveguide width (d) is compared with measured data, we demonstrate the agreement between the waveguide model and the experimental data. For the evanescent modes ($\nu < \nu_c$) the attenuation of the waveguide strongly increases with its length. A long waveguide (i.e., thick aperture) will strongly attenuate spectral content below the cutoff frequency, thus temporally modulating the diffracted radiation. At the same time, a thin aperture has much lower attenuation across the same spectral region, allowing for little or no temporal change in the output pulse. Indeed, the transmission function falls off slowly below the roll-off frequency $\nu_r \sim 1.5\,c/\pi d$.[22]

5. COMPARISON OF THICK AND THIN APERTURES

We now return to the comparison of thin and thick apertures by studying the diffraction and propagation of THz pulses, using the FDTD algorithm. Figure 7 compares the propagation of the TM half-cycle pulse through thin (left column) and thick (right column) apertures. The instantaneous amplitude of the electric field is plotted at three consecutive times: (top) the TM half-cycle pulse starts to penetrate the 500-μm-wide and 1.7-mm-thick aperture (18.75 ps), (middle) the pulse emerges from the thick aperture (26.25 ps), and (bottom) the pulse is fully transmitted though the aperture (33.75 ps) and begins to diffract into the half-space past the aperture. The on-axis amplitude profile is plotted in each case and clearly indicates strong temporal shaping within the thick aperture itself. It also shows a comparatively small change in the shape of the pulse transmitted by a thin aperture. It is important to notice that the temporal shape of the diffracted radiation does not change significantly as we move the observation point off axis. Indeed, an extensive set of FDTD calculations was performed to test this conclusion. We found that the only significant difference between on- and off-axis diffracted signal exists in the near-dc region. Weak spectral features (~12 dB below the cutoff-frequency spectral strength) positioned at multiples of the cutoff frequency are also seen. The role of the increasing aperture thickness in the pulse reshaping is illustrated in Fig. 8. The incident half-cycle TM pulse is completely diffracted by the thin aperture ($d = 283\ \mu$m), suffering negligible temporal modulation after $t = 18$ ps. When it is incident upon the thick aperture ($d = 1698\ \mu$m), on the other hand, the incident pulse is just beginning a reshaping process during the same 18-ps time delay.

The value of the cutoff frequency ($\nu_c = c/2d$) is precisely controlled by the aperture width d. Figure 9 illustrates this point for varying aperture widths with the aperture thickness kept constant ($l = 1.7$ mm). A higher cutoff frequency (narrower aperture width) attenuates a broader portion of the incident pulse spectrum. This process ultimately leads to formation of the carrier-frequency pulse, whose spectral spread rapidly narrows with the increase in the cutoff frequency. For a very narrow aperture width ($d = 300\ \mu$m) the corresponding cutoff frequency is 0.5 THz, and the transmitted pulse closely

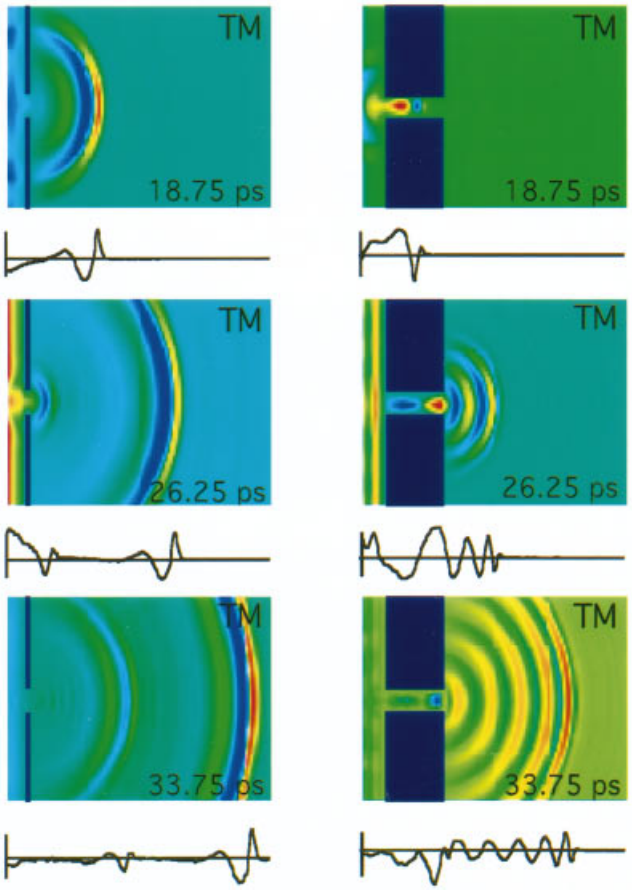

Fig. 7. TM diffraction: thin (left, $l = 0.1$ mm) versus thick (right, $l = 1.7$ mm) conductive apertures. The aperture width is $d = 0.5$ mm in both cases.

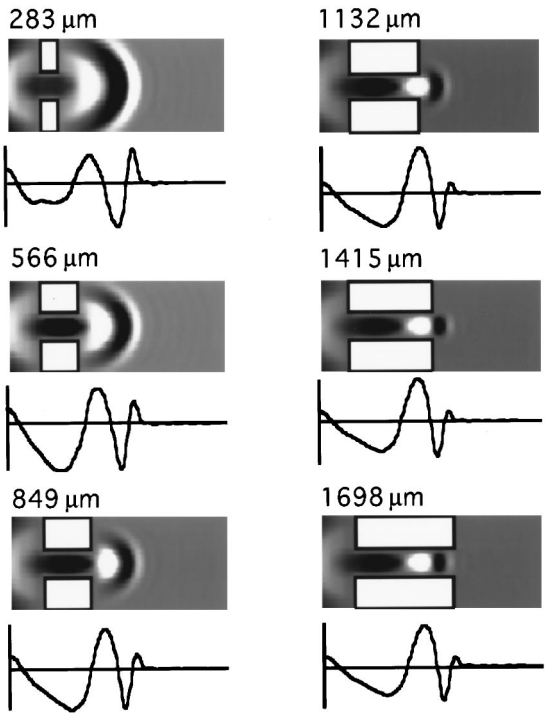

Fig. 8. TM pulse shaping in variable-thickness conductive apertures: the 0.5-mm-wide aperture thickness is increased from 283 μm (thin) to 1698 μm (thick).

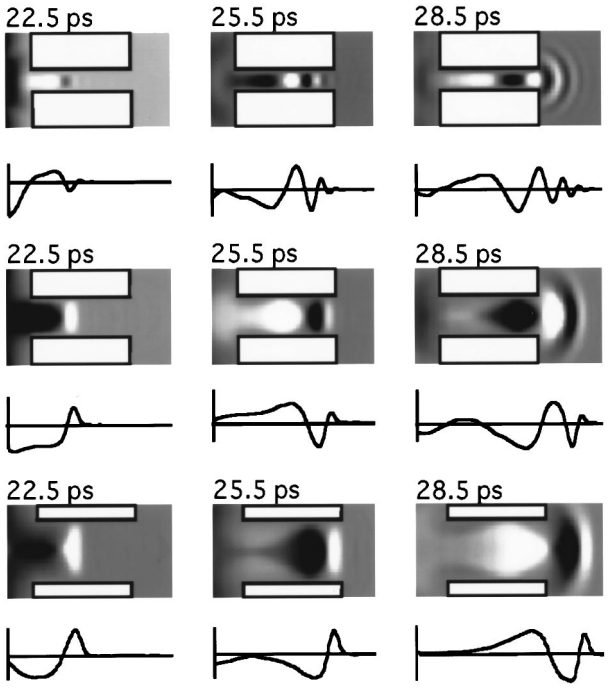

Fig. 9. TM pulse shaping in variable-width apertures: the 1.7-mm-thick aperture width is 300 μm (upper row), 700 μm (middle row), and 1100 μm (bottom row).

resembles the carrier-frequency form. The diffraction from the wide aperture (d = 1100 μm) with a cutoff frequency of 0.136 THz results in an almost half-cycle pulse shape. We emphasize the importance of this mechanism for any applications that require carrier UWB radiation (e.g., UWB ranging and sensing).

6. CONCLUSION

We have developed a simple quasi-optical technique for passive spatiotemporal reshaping of half-cycle THz radiation. We have demonstrated that a conductive aperture can be used to control precisely the form of an incident half-cycle pulse. The conductive slit geometry (slit width and thickness) and pulse polarization are used to convert the incident half-cycle radiation into the carrier-frequency signal. Although free-space propagation can also be used to attenuate low-frequency spectral content, our method offers a much more discriminative and precise spectral control. Temporal modulation of the transmitted radiation is shown to be a dominant effect in all the geometries considered and is approximately identical along any azimuthal direction. The latter observation allows the simple waveguide model, used for the on-axis filter response, to be used throughout the entire half-space past the aperture.

This simple demonstration of a quasi-optical slit filter and the power and accuracy of the FDTD simulations shows the possibility of synthesis of custom filters. Many of the techniques used in the microwave domain could be scaled down to the THz domain.[23] Possibilities include using the reflected low-frequency component of the pulse or designing tapered filters (in which the cutoff frequency varies with position inside the waveguide), arrays of slit filters, and three-dimensional apertures.

ACKNOWLEDGMENT

This research was supported in part by the U.S. Army Research Office and by the National Science Foundation under contracts ECS-9413989 and PHY 94-15583.

REFERENCES

1. A. Baltuska, Z. Wei, M. Pshenichnikov, and D. Wiersma, "Optical pulse compression to 5 fs at a 1-MHz repetition rate," Opt. Lett. **22**, 102 (1997).
2. R. L. Fork, C. H. Brito Cruz, P. C. Becker, and C. V. Shank, "Compression of optical pulses to six femtoseconds by using cubic phase compensation," Opt. Lett. **12**, 483 (1987).
3. D. H. Auston, K. P. Cheung, and P. R. Smith, "Picosecond photoconducting Hertzian dipoles," Appl. Phys. Lett. **45**, 284 (1984).
4. D. R. Dykaar, B. I. Greene, J. F. Federici, A. F. J. Levi, L. N. Pfeiffer, and R. F. Kopf, "Log-periodic antennas for pulsed terahertz radiation," Appl. Phys. Lett. **59**, 262 (1991).
5. J. T. Darrow, B. B. Hu, X.-C. Zhang, and D. H. Auston, "Subpicosecond electromagnetic pulses from large-aperture photoconducting antennas," Opt. Lett. **15**, 323 (1990).
6. X.-C. Zhang, B. B. Hu, J. T. Darrow, and D. H. Auston, "Generation of femtosecond electromagnetic pulses from semiconductor surfaces," Appl. Phys. Lett. **56**, 1011 (1990).
7. L. Xu, X.-C. Zhang, D. H. Auston, and B. Jahali, "Terahertz radiation from large aperture Si p-i-n diodes," Appl. Phys. Lett. **59**, 3357 (1991).
8. X.-C. Zhang, B. B. Hu, S. Xin, and D. H. Auston, "Optically induced femtosecond electromagnetic pulses from GaSb/AlSb strained-layer superlattice," Appl. Phys. Lett. **57**, 753 (1990).
9. A. S. Weling, B. B. Hu, N. M. Froberg, and D. H. Auston, "Generation of tunable narrow-band THz radiation from large aperture photoconducting antennas," Appl. Phys. Lett. **64**, 137 (1994).
10. S. R. Keiding, "THz spectroscopy in atomic, molecular and

optical physics," Comments At. Mol. Phys. **30**, 37 (1994).
11. B. B. Hu and M. C. Nuss, "Imaging with terahertz waves," Opt. Lett. **20**, 1716 (1995).
12. R. R. Jones, "Creating and probing electronic wave packets using half-cycle pulses," Phys. Rev. Lett. **76**, 3927 (1996).
13. R. Cheville, B. Nicholson, and D. Grischkowsky, "Compact time-domain terahertz ranging system," in *Conference on Lasers and Electro-Optics*, Vol. 15 of 1995 OSA Technical Digest Series (Optical Society of America, Washington, D.C., 1995), p. 360.
14. J. Wenbin, S. Diechi, and L. Fuming, "Distortion of femtosecond optical pulses with Gaussian spatial distribution propagating in free space," Chin. Phys. **10**, 168 (1990).
15. D. You and P. H. Bucksbaum, "Propagation of half-cycle FIR pulses," J. Opt. Soc. Am. B **14**, 1651 (1997).
16. N. M. Froberg, B. B. Hu, X.-C. Zhang, and D. H. Auston, "Terahertz radiation from a photoconducting antenna array," IEEE J. Quantum Electron. **28**, 2291 (1992).
17. J. O. White, C. Ludwig, and J. Kuhl, "Response of grating pairs to single-cycle electromagnetic pulses," J. Opt. Soc. Am. B **12**, 1687 (1995).
18. J. T. Darrow, D. H. Auston, and J. Morse, "Large-aperture photoconducting antennas excited by high optical fluences," in *Ultrafast Pulse Generation and Spectroscopy*, T. R. Gosnell, A. J. Taylor, K. A. Nelson, and M. C. Downer, eds., Proc. SPIE **1861**, 186 (1993).
19. A. Taflove, *Computational Electrodynamics: The Finite-Difference Time-Domain Method* (Artech, Norwood, Mass., 1995).
20. A. Taflove and M. Brodwin, "Numerical solution of steady-state electromagnetic scattering problems using the time-dependent Maxwell's equations," IEEE Trans. Microwave Theory Tech. **MTT-23**, 623 (1975).
21. R. Collin, *Foundations for Microwave Engineering* (McGraw-Hill, New York, 1992).
22. J. S. Asvestas and R. E. Kleinman, in *Electromagnetic and Acoustic Scattering by Simple Shapes*, J. J. Bowman, T. B. A. Senior, and P. L. E. Uslenghi, eds. (North-Holland, Amsterdam, 1969), Chap. 4, pp. 181–239.
23. R. H. Garnham, in *Millimetre and Submillimetre Waves*, F. A. Benson, ed. (Iliffe, London, 1969), Chap. 21, pp. 403–450.